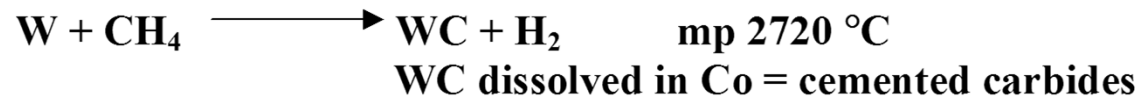
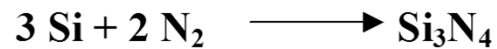
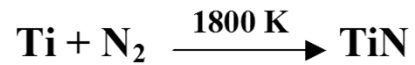


Gas Phase Reactions

Heating: furnace, laser, plasma, flame, arc

Gas-Metal Rxn



cementite



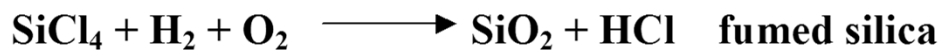
Gas Phase Reactions

Gas-Gas Rxn

homogeneous nucleation from supersaturated vapor (nano)

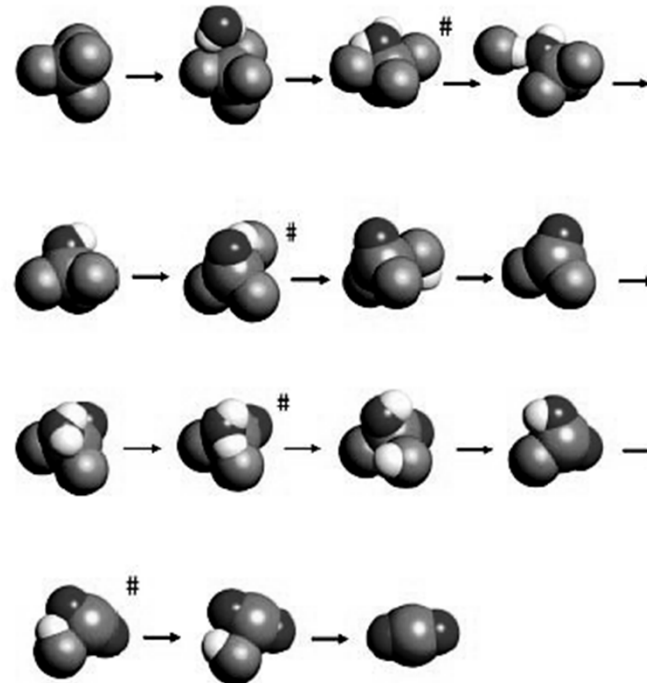
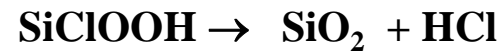
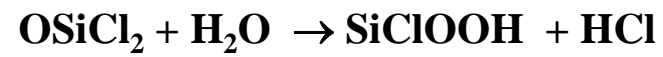
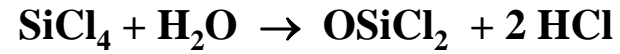
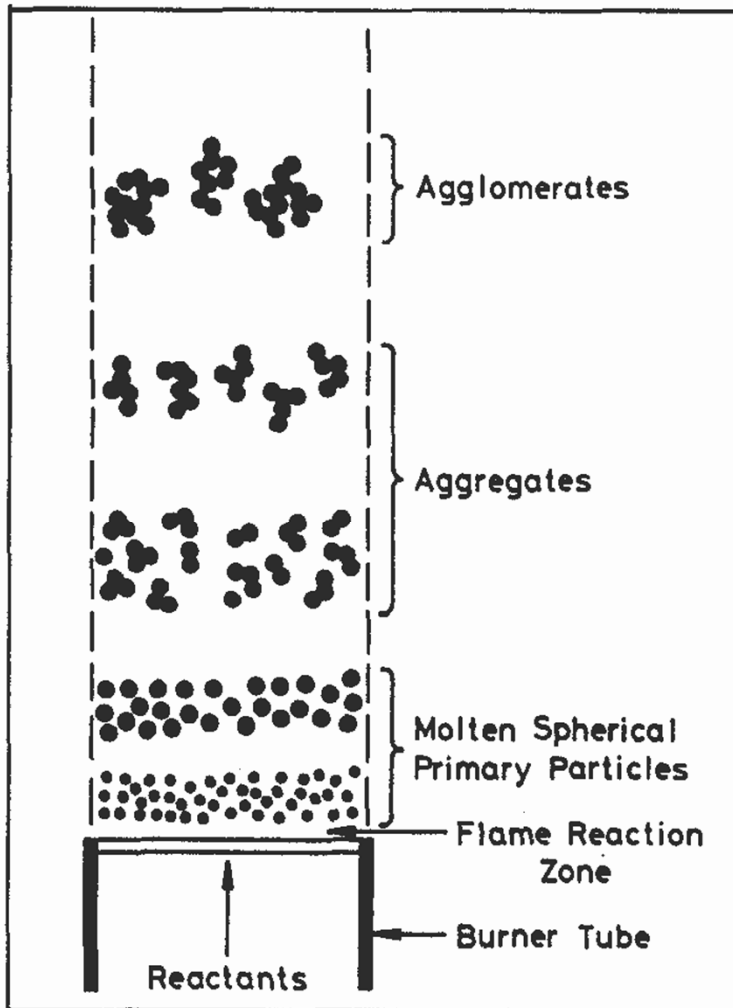
Flame hydrolysis

volatile compounds are passed through an oxygen-hydrogen stationary flame:

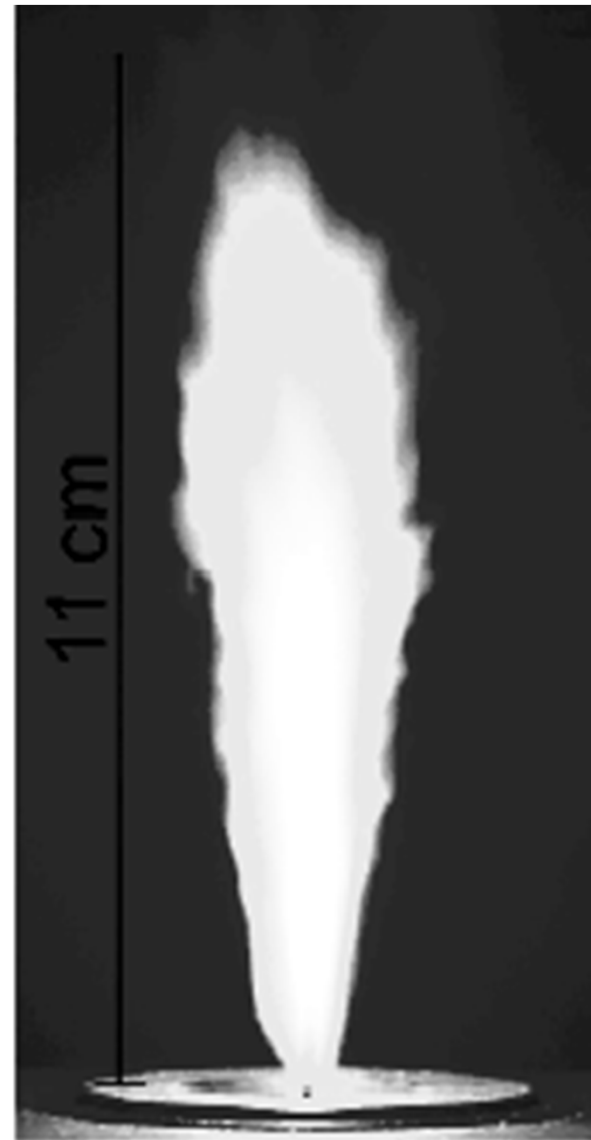
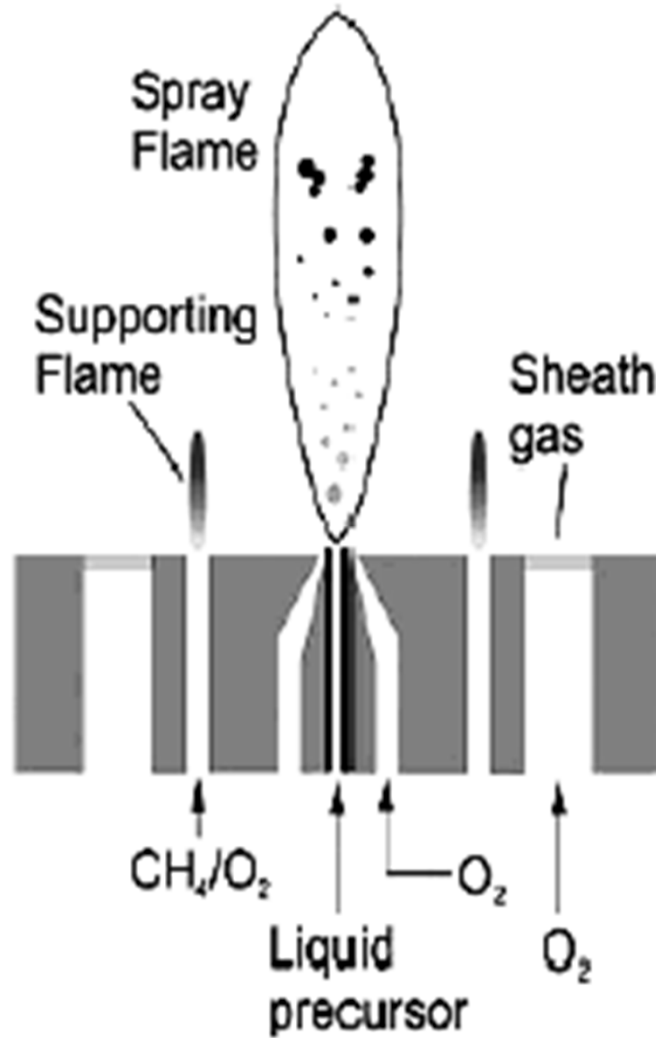


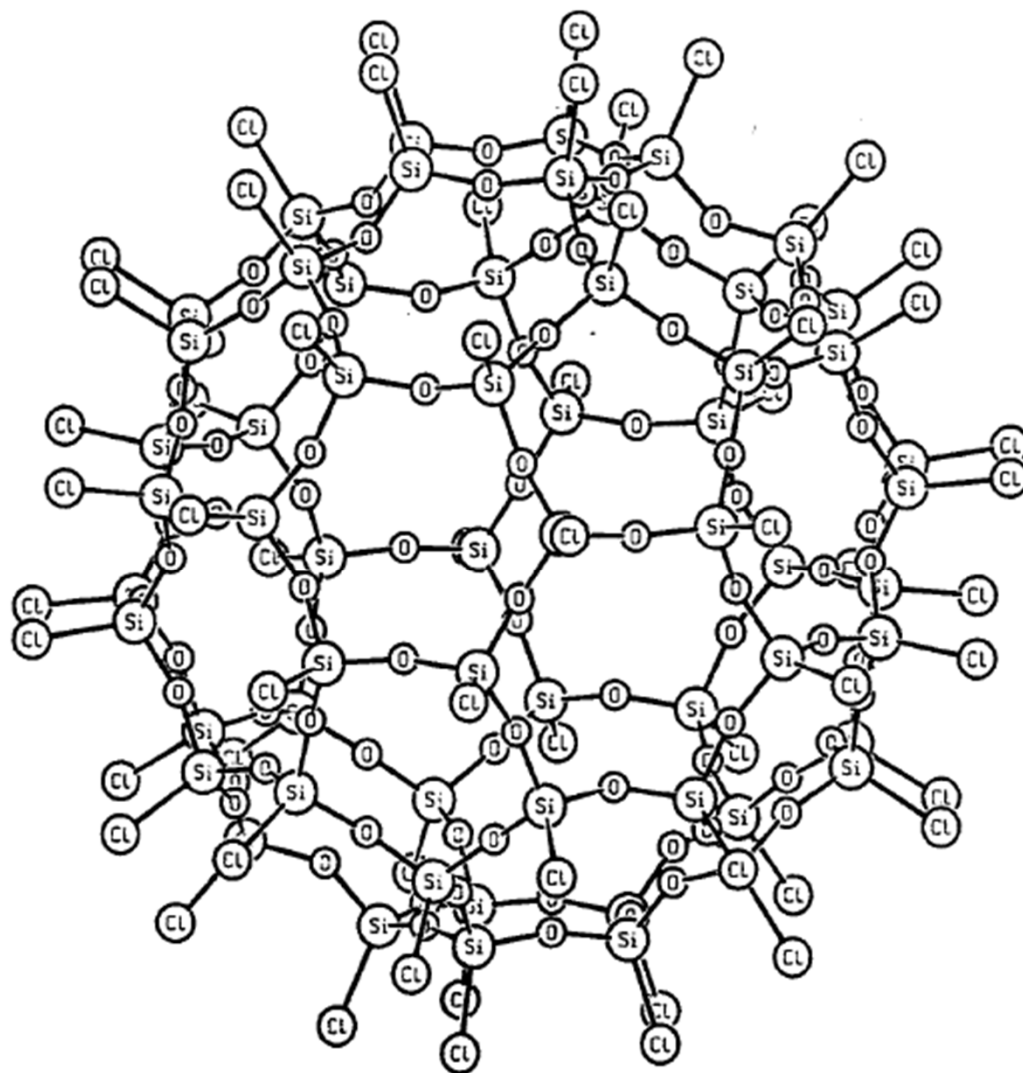
reagent	bp/°C	product
SiCl ₄	57	SiO ₂
AlCl ₃	180 (subl.)	Al ₂ O ₃
TiCl ₄	137	TiO ₂
CrO ₂ Cl ₂	117	Cr ₂ O ₃
Fe(CO) ₅	103	Fe ₂ O ₃
GeCl ₄	84	GeO ₂
Ni(CO) ₄	42	NiO
SnCl ₄	114	SnO ₂
ZrCl ₄	331 (subl.)	ZrO ₂
VOCl ₃	127	V ₂ O ₅

Gas Phase Reactions



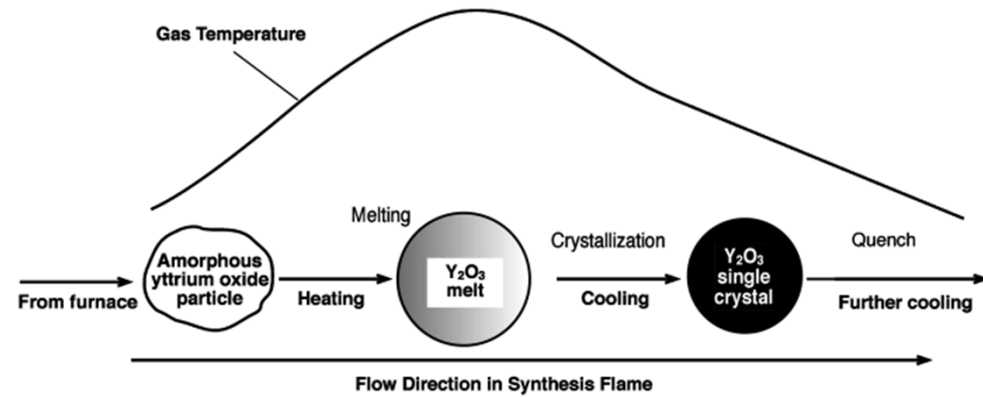
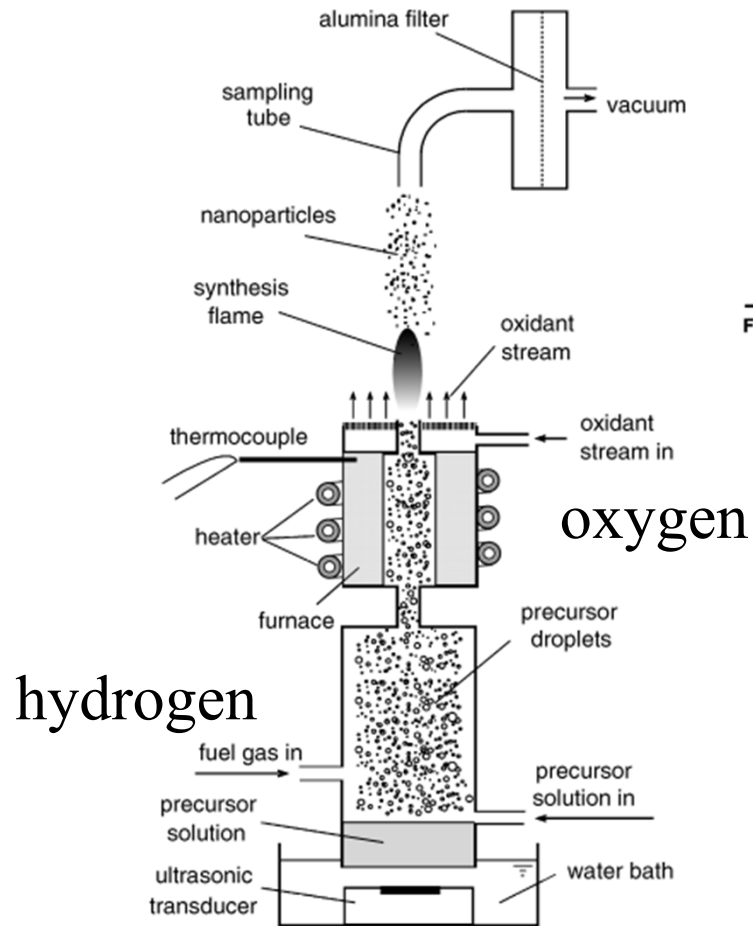
Gas Phase Reactions





Si₆₀O₉₀Cl₆₀ (*I_h*)

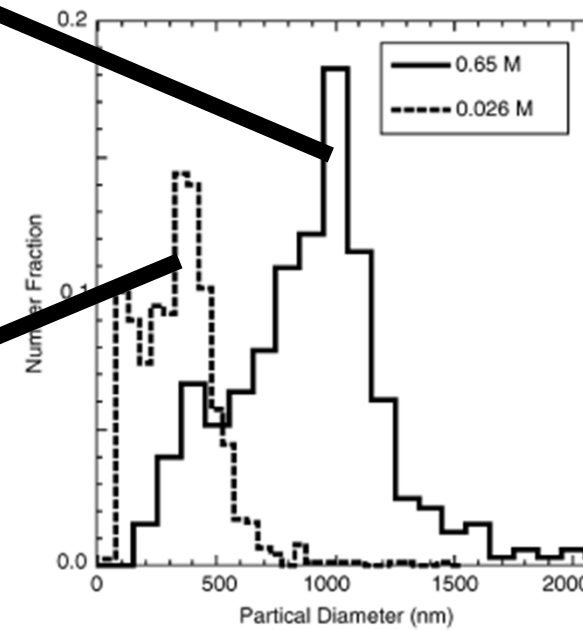
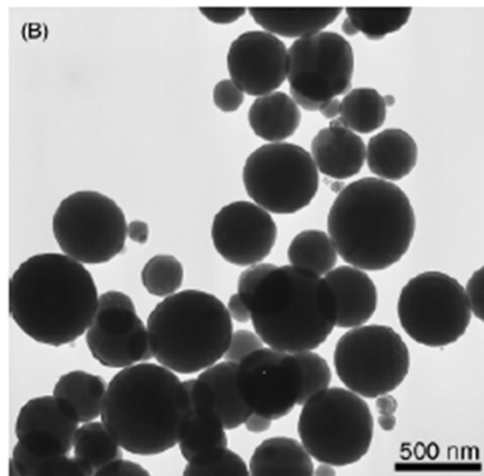
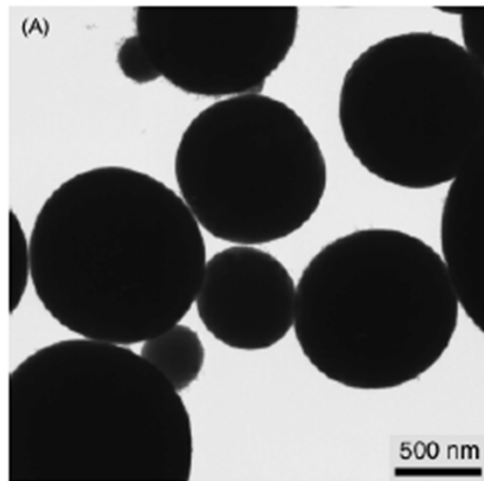
Y₂O₃ Particles by Flame Aerosol Process



Particle Size Control

Particle size control by precursor concentration

Higher concentration = larger size



Gas Phase Reactions

Calcium phosphate nanoparticles Ca/P molar ratios 1.43 to 1.67

**synthesized by simultaneous combustion of
 $\text{Ca}(\text{OAc})_2 + \text{OP}(\text{O}^n\text{Bu})_3$ in a flame spray reactor**

**Fluoro-apatite and zinc or magnesium doped calcium phosphates
adding trifluoroacetic acid or metal carboxylates into the fuel.**

Nanoparticle morphology

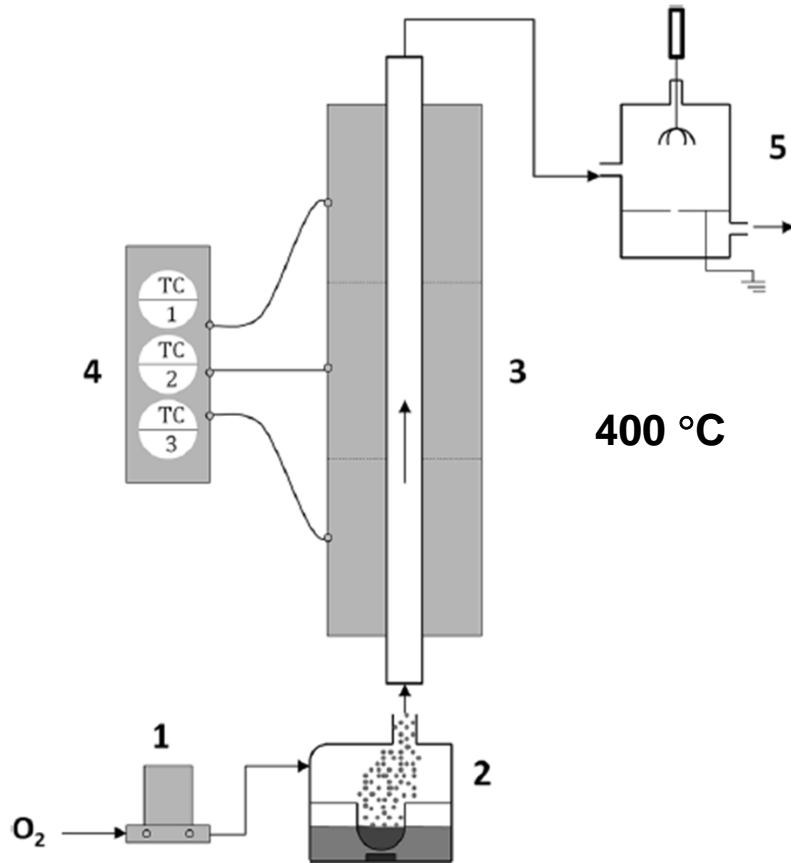
**At a molar ratio of $\text{Ca}/\text{P} < 1.5$ promoted the formation of dicalcium pyrophosphate
($\text{Ca}_2\text{P}_2\text{O}_7$).**

**Phase pure tricalcium phosphate TCP - $\text{Ca}_3(\text{PO}_4)_2$
obtained with a precursor Ca/P ratio of 1.52 after subsequent calcination at 900 °C**

**micropores and the facile substitution of both anions and cations
possible application as a biomaterial.**

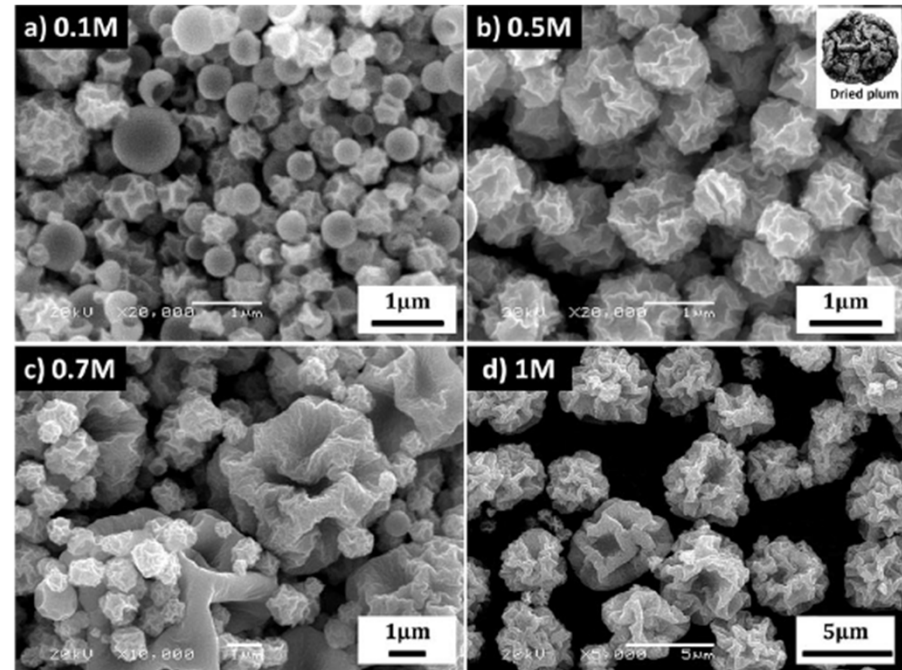
Spray Pyrolysis

tubular furnace reactor

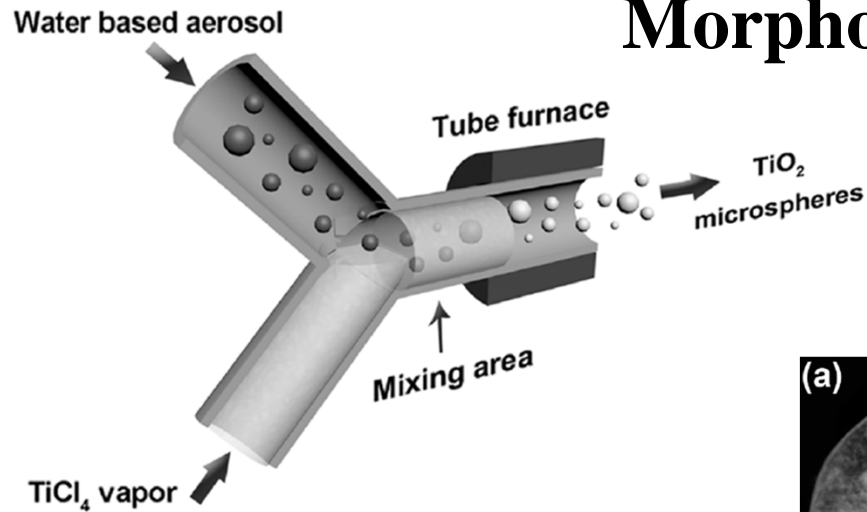


- (1) mass flow controller – O₂ 1 L/min
- (2) ultrasonic nebulizer – aqueous solution
2 Co(OAc)₂ : 1 Ni(OAc)₂
- (3) 3-zone heater - 400 °C
- (4) temperature controller
- (5) electrostatic precipitator

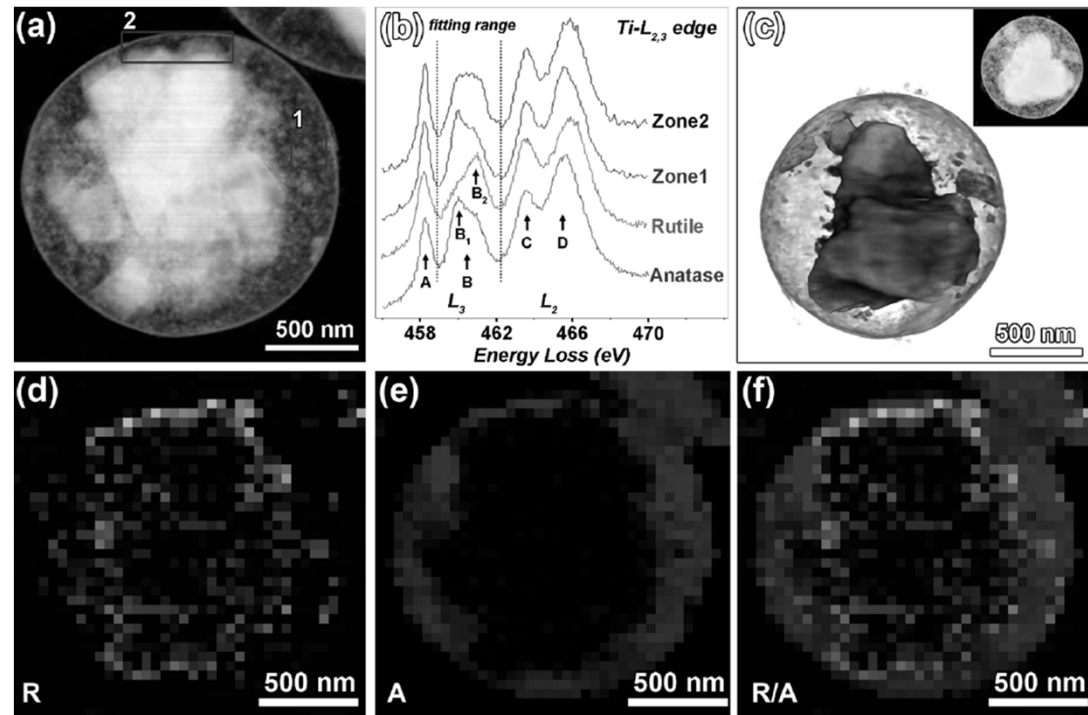
SEM micrographs of NiCo₂O₄ particles obtained from different concentrations of Co(OAc)₂ and Ni(OAc)₂ precursor solutions – Lower concentration reduces particle size



Morphology Control

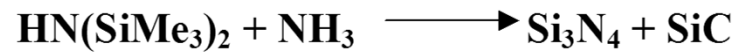
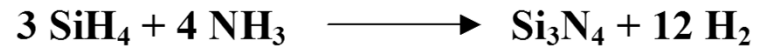


(a) HAADF-STEM of a rutile@anatase core@shell microspheres; (b) titanium L_{2,3} core-loss EELS spectra acquired from the indicated areas compared to reference TiO₂ polymorphs [rutile (green) and anatase (red)] (d–f) EELS maps: (d) rutile (green), (e) anatase (red), and (f) rutile and anatase overlaid color map. (c) 3D tomographic reconstruction of another typical rutile@anatase core-shell microspheres, together with the corresponding HAADF-STEM image (inset).

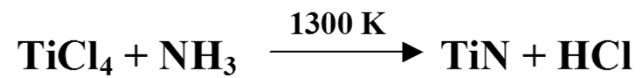


Gas Phase Reactions

High-power CO₂ lasers



DC-Ar Plasma



Tarnishing of Metal Surfaces

oxide, hydroxide layers

Arc



Vapor Phase Transport Syntheses

Sealed glass tube reactors

Solid reactant(s) A + gaseous transporting agent B

Temperature gradient furnace $\Delta T \sim 50^\circ\text{C}$

Equilibrium established $\text{A(s)} + \text{B(g)} \leftrightarrow \text{AB(g)}$

Equilibrium constant K

A + B react at T_2

Gaseous transport by AB(g)

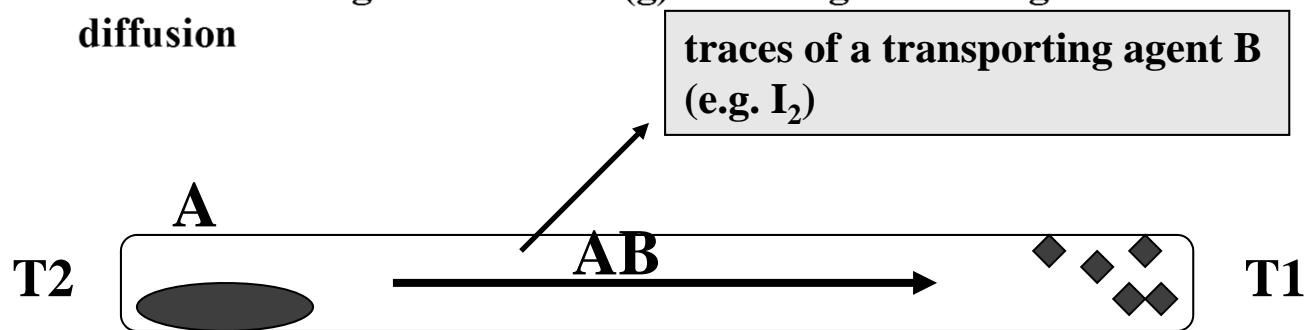
AB(g) decomposes back to A(s) at T_1 , crystals of pure A

Temperature dependent K

Equilibrium concentration of AB(g) changes with T

Different at T_2 and T_1

Concentration gradient of AB(g) = driving force for gaseous diffusion



Vapor Phase Transport Syntheses

Whether $T_1 < T_2$ or $T_1 > T_2$ depends on the thermochemical balance of the reaction !
Transport can proceed from higher to lower or from lower to higher temperature

Example: $\text{Pt(s)} + \text{O}_2(\text{g}) \leftrightarrow \text{PtO}_2(\text{g})$

Endothermic reaction, PtO_2 forms at hot end, diffuses to cool end, deposits well formed Pt crystals, observed in furnaces containing Pt heating elements

Chemical vapor transport, $T_2 > T_1$, provides concentration gradient and thermodynamic driving force for gaseous diffusion of vapor phase transport agent AB(g)

Uses of VPT

- synthesis of new solid state materials
- growth of single crystals
- purification of solids

Vapor Phase Transport Syntheses

Thermodynamics of VPT

Reversible equilibrium needed: $\Delta G^\circ = -RT \ln K_{\text{equ}} = \Delta H^\circ - T\Delta S^\circ$

✎ Exothermic $\Delta H^\circ < 0$

Smaller T implies larger K_{equ}

AB forms at cooler end, decomposes at hotter end of reactor



✎ Endothermic $\Delta H^\circ > 0$

Larger T implies larger K_{equ}

AB forms at hotter end, decomposes at cooler end of reactor



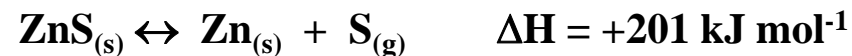
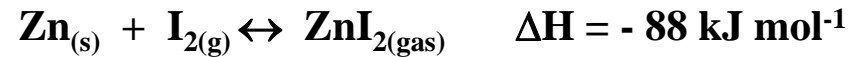
van't Hoff equation

$$\ln K_2 - \ln K_1 = \ln \frac{K_2}{K_1} = \frac{\Delta H^\circ}{R} \left(\frac{1}{T_1} - \frac{1}{T_2} \right)$$

Vapor Phase Transport Syntheses

Estimation of the thermochemical balance (ΔH) of a transport reaction:

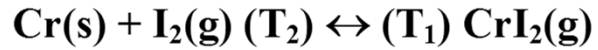
e.g.:



endothermic reaction, transport from hot to cold!

Applications of VPT Methods

☛ Purification of Metals: Van Arkel Method



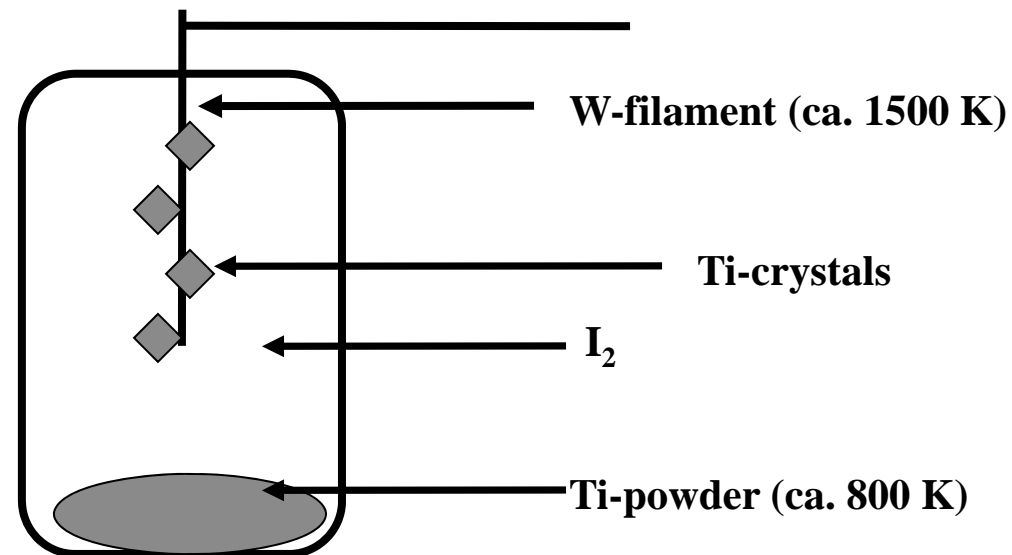
Exothermic, $\text{CrI}_2(\text{g})$ forms at T_1 , pure Cr(s) deposited at T_2

Useful for Ti, Hf, V, Nb, Cu, Ta, Fe, Th

Removes metals from carbide, nitride, oxide impurities



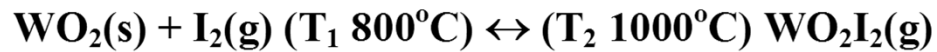
exothermic: transport from cold to hot



Applications of VPT Methods

☛ Double Transport Involving Opposing Exothermic-Endothermic Reactions

Endothermic:



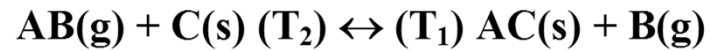
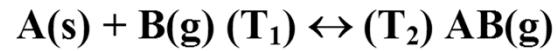
Exothermic:



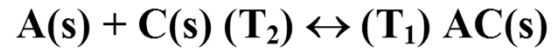
The antithetical nature of these two reactions allows W/WO₂ mixtures to be separated at different ends of the gradient reactor using H₂O/I₂ as the transporting VP reagents

Applications of VPT Methods

☛ Vapor Phase Transport for Synthesis



Concept: couple VPT with subsequent reaction to give overall reaction:

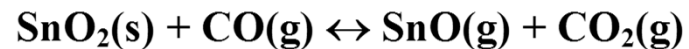


Examples:

Direct reaction sluggish even at high T

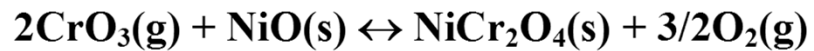
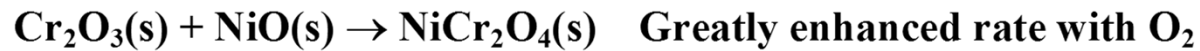


Useful phosphor, greatly speeded up with CO as VPT agent:



Applications of VPT Methods

Direct Reaction:

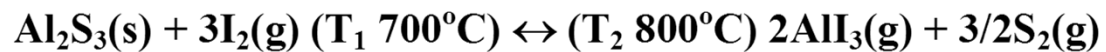


Overcoming Passivation Through VPT



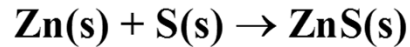
In presence of cleansing VPT agent I₂:

Endothermic:



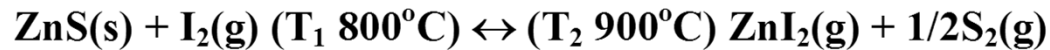
Applications of VPT Methods

●* Vapor Phase Transport for Synthesis



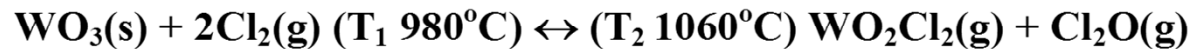
passivation prevents reaction to completion

Endothermic:



VPT Synthesis of ZnWO₄:

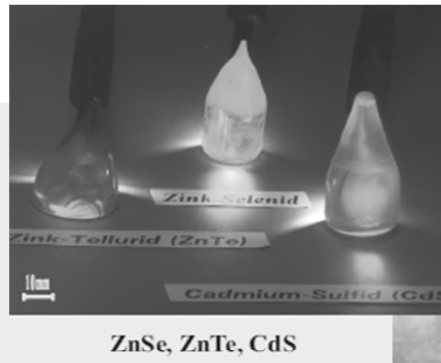
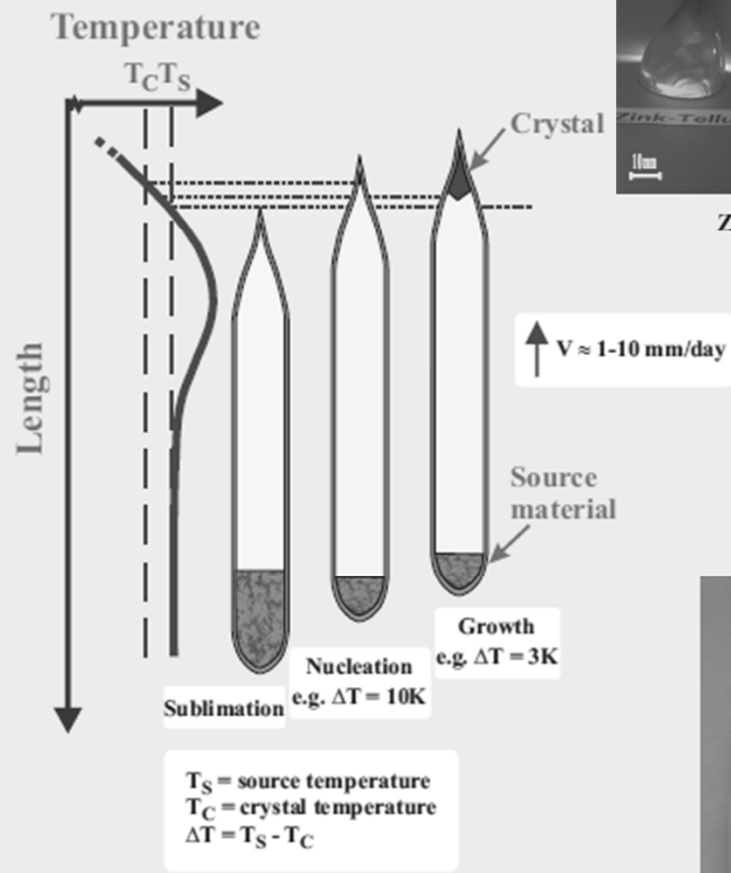
A Real Phosphor Host Crystal for Ag⁺, Cu⁺, Mn²⁺



Growing Epitaxial GaAs Films by VPT Using Convenient Starting Materials



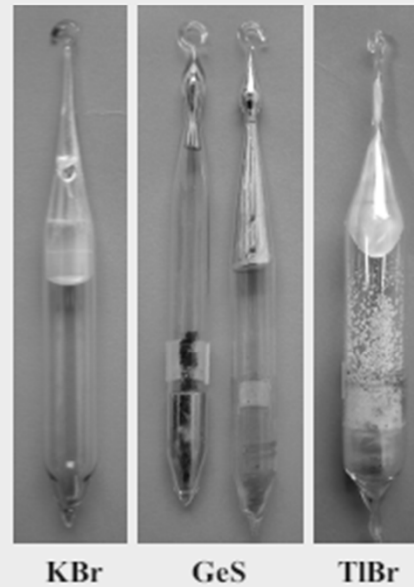
Serves to establish initial equilibrium



1. Purification by sublimation
2. Synthesis
3. Sublimation or chemical vapor transport

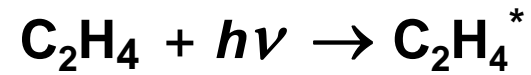
Crystals grown:

ZnO, ZnSe, ZnTe, CdS,
 CdSe, Ag_2S , CuCl, CuBr,
 CuI, AgI, TiO_2 , C_{60} , C_{70} ,
 Zn, Cd, Mg etc.



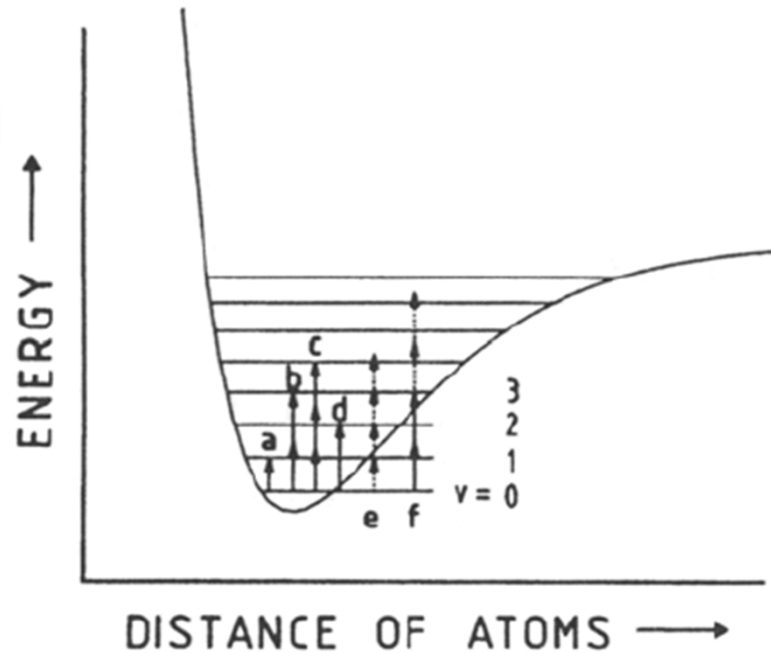
A view of vapor growth equipment

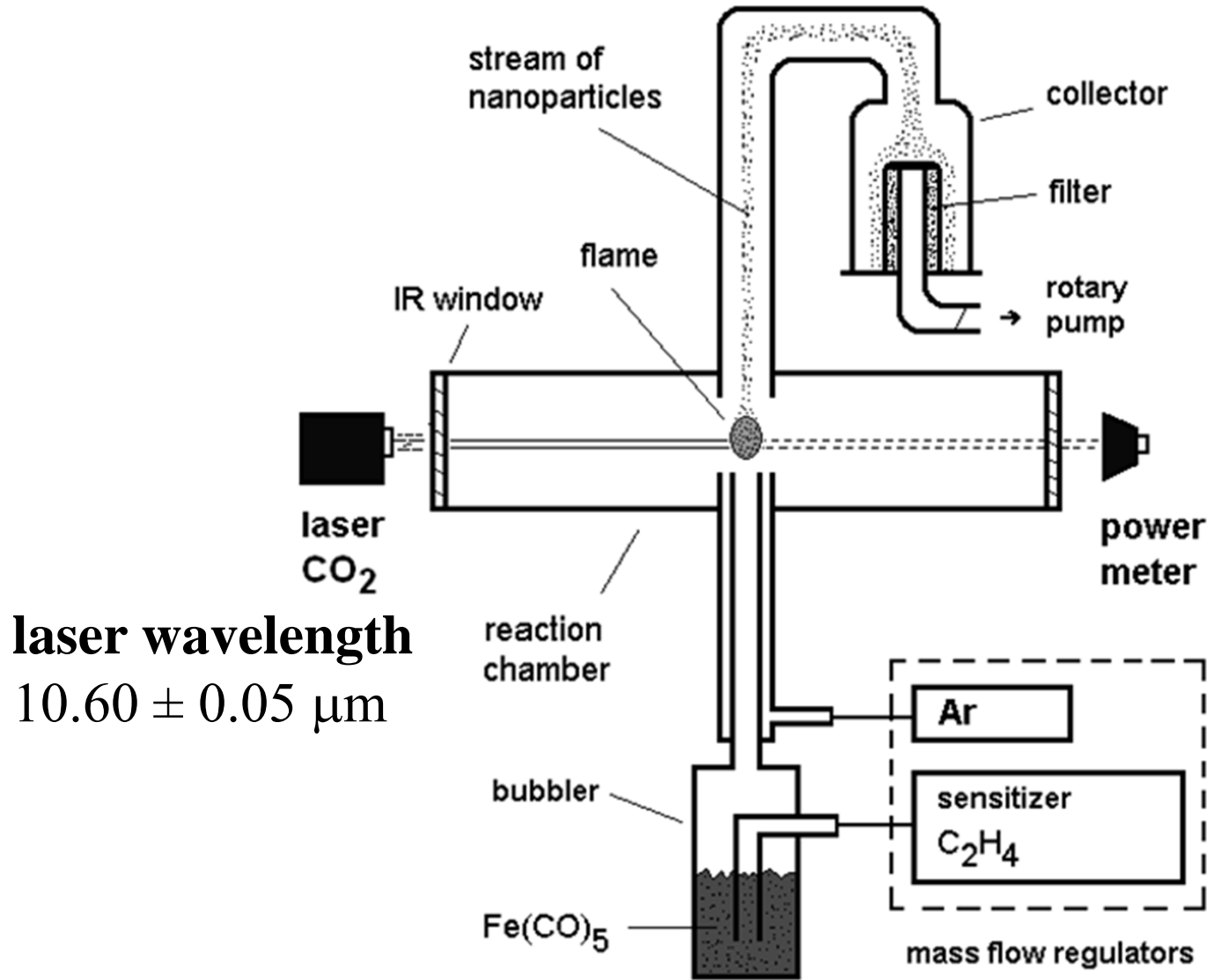
Laser-induced homogeneous pyrolysis, LIHP



Excitation energy transferred to
vibrational-translational modes

⇒ T increases





laser wavelength
 $10.60 \pm 0.05 \mu\text{m}$

Sensitizer

SF₆
 948 cm^{-1}

Isopropanol
 958 cm^{-1}

Reaction Zone

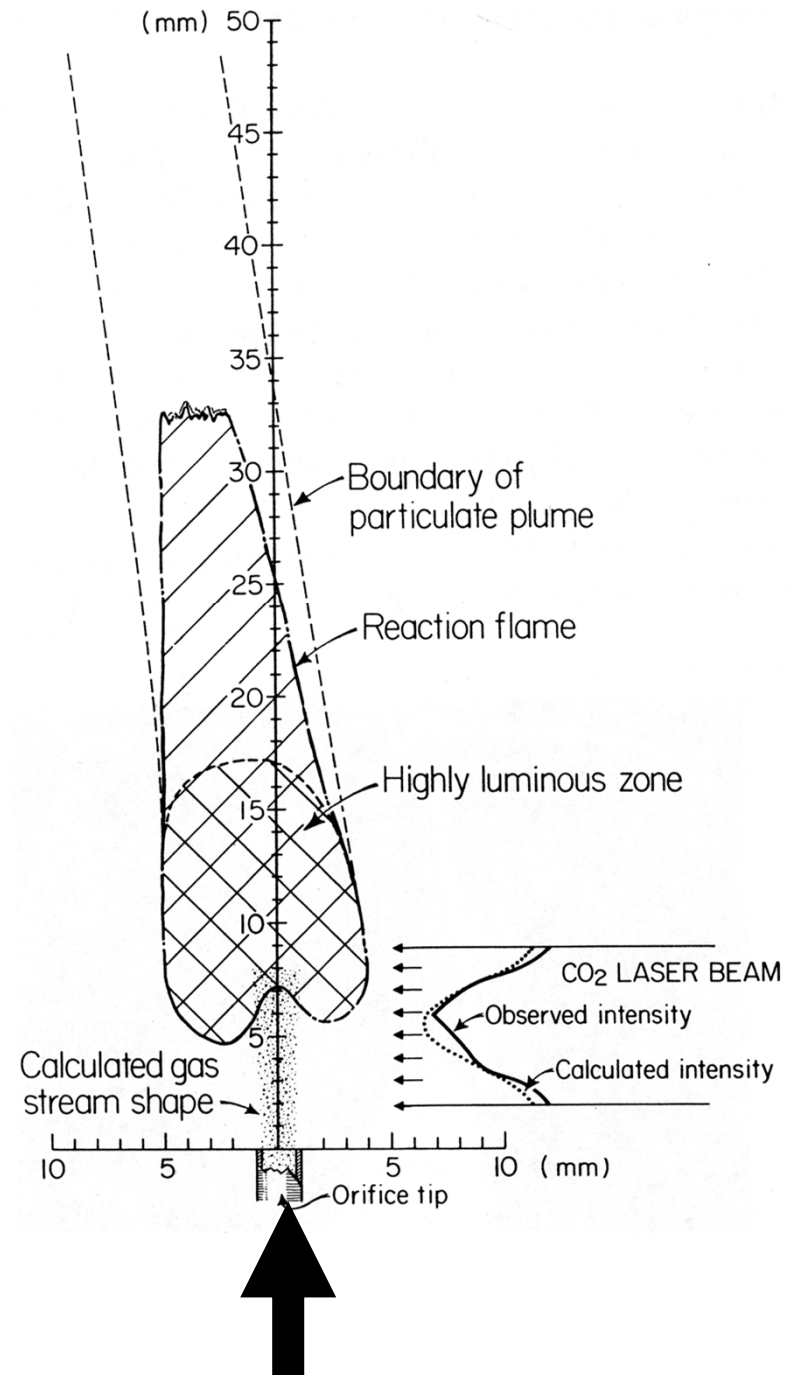
Overlap between
the vertical reactant gas stream
and the horizontal laser beam

away from the chamber walls

nucleation of nanoparticles

less contamination

narrow size distribution



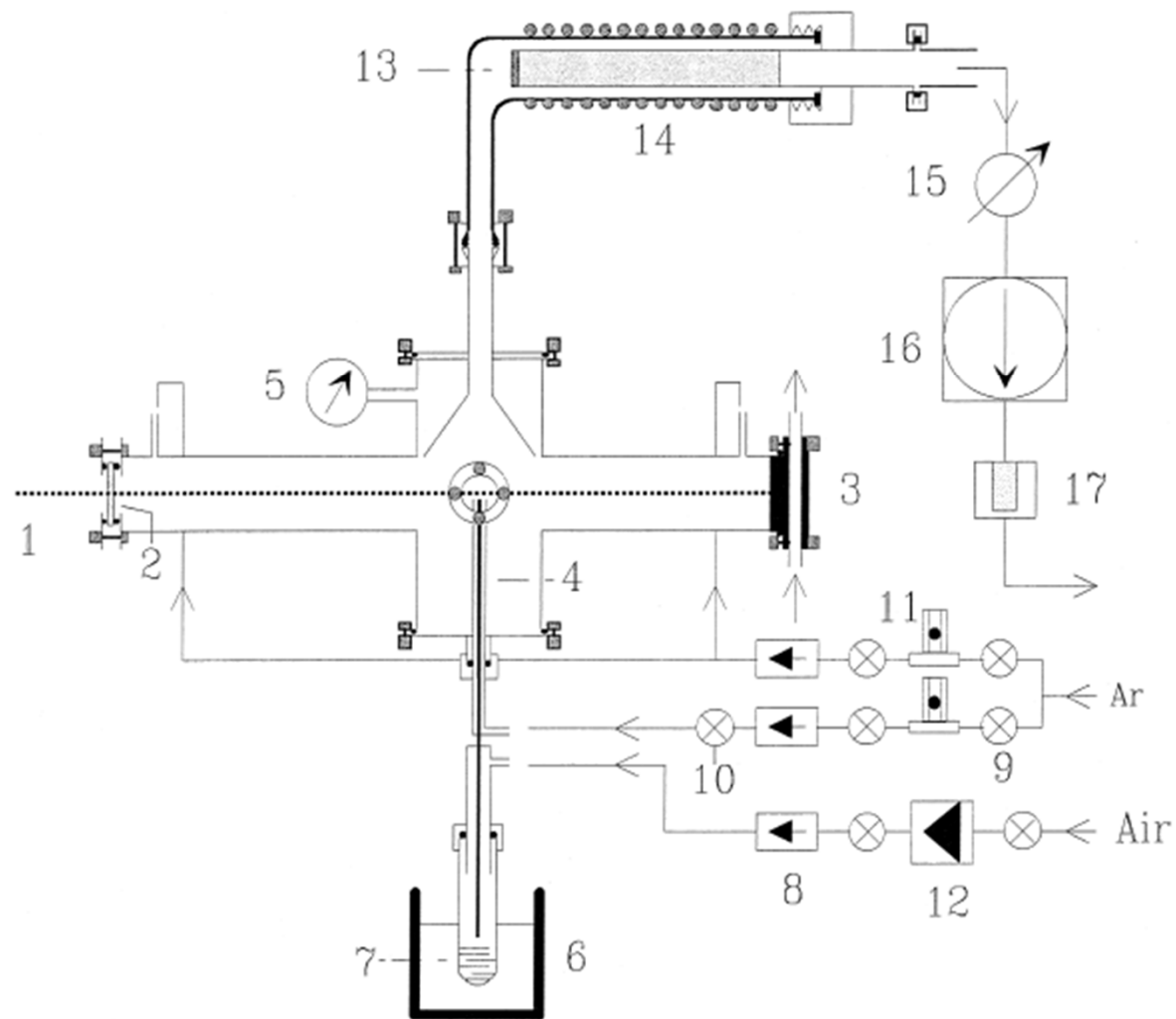
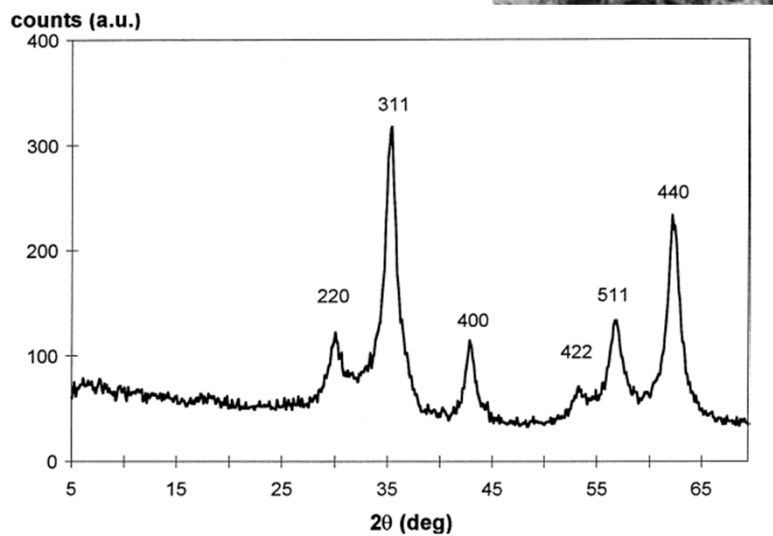
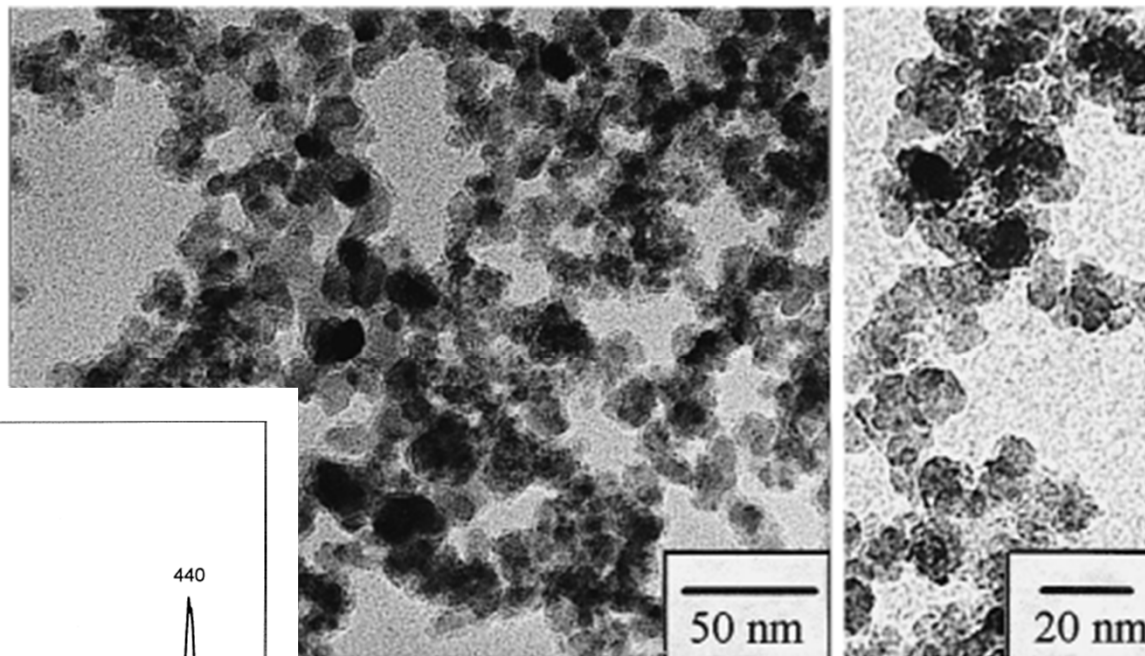
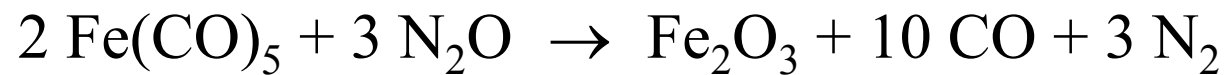


Fig. 1. CO₂ laser pyrolysis system. (1) Laser beam, (2) ZnSe window, (3) water refrigerated aluminium target, (4) nozzle, (5) pressure gauge, (6) ultrasonic bath, (7) 30% iron pentacarbonyl solution in isopropanol, (8) not return valve, (9) ball valve, (10) three ways ball valve, (11) argon rotameter, (12) massic controller of air flux, (13) stainless steel filter to collect the produced powders, (14) heating resistance, (15) pressure controller valve, (16) rotary vacuum pump, (17) filter to capture oil mist.

Iron-oxide Nanoparticles by Laser-induced Pyrolysis



TEM micrographs of the synthesised $\gamma\text{-Fe}_2\text{O}_3$ particles.